

FIBERTUNE: Preserving Action-Fiber Visual Residuals in Vision-Language-Action Fine-Tuning

Haihao Lin^{1*} Xiangsheng Huang² Xiao Yang¹ Weibang Zhou¹
Yiqi Zhang³ Bo Yang³ Simin Zeng¹ Jiawei Yang⁴
Zhengyang Wang⁴ Jiahui Du⁴

¹University of Chinese Academy of Sciences

²Hebei Key Laboratory of Cognitive Intelligence, Xiong'an Institute of Innovation

³Hebei University of Technology ⁴Beijing Information Science and Technology University

Abstract: Action-supervised fine-tuning of VLA policies fits demonstrations effectively but constrains only the directions that change predicted actions, leaving visual structure consistent across action-equivalent states free to collapse. We formalize this as residual visual collapse along local action fibers and propose FIBERTUNE, a training-time objective that preserves teacher-structured visual residuals without adding inference-time overhead. FIBERTUNE uses an online action probe to estimate action-predictive feature directions, filters them from intermediate visual-token representations, and aligns the resulting probe-filtered residuals to a frozen visual teacher while regularizing their effective rank. Under identical training conditions, FIBERTUNE improves over task-loss-only fine-tuning in every one of six controlled simulation settings spanning two benchmarks and two architectures ($\pi_{0.5}$ and OpenVLA-OFT), as well as on physical SO-101 pick-place; representative gains include +10.7 pp SR(5) on long-horizon CALVIN ABC \rightarrow D and physical SO-101 task success rising from 72.7% to 78.1%. Residual diagnostics show that these gains coincide with increased probe-filtered residual teacher alignment and effective rank, consistent with the action-fiber motivation.

Keywords: Vision-Language-Action Models, Representation-Preserving Fine-Tuning, Robot Manipulation

1 Introduction

Language-conditioned robot learning has progressed from grounding language in affordances, task-conditioned imitation, and multimodal prompts to modern VLA policies that directly map observations and instructions to robot actions [1, 2, 3, 4]. Large VLA policies such as RT-1, RT-2, RoboFlamingo, OpenVLA, OpenVLA-OFT, Octo, CogACT, and π_0 -style policies have made it practical to adapt pretrained visual and language representations to robot control through action-supervised fine-tuning [5, 6, 7, 8, 9, 10, 11, 12, 13]. This adaptation is central to modern robot learning, but action-supervised losses constrain only the directions that change predicted actions — visual factors consistent across action-equivalent states receive no direct gradient and can compress during fine-tuning. For example, color, category, background, nearby distractors, or future-relevant object state can be visually meaningful while requiring the same short-horizon end-effector command.

We formalize this through local *action fibers*: for a supervised action target a , the action fiber is the set of representations that produce the same prediction under h_θ ; action loss constrains directions that cross fibers but leaves fiber-tangent directions — where action-equivalent visual structure lives — without direct gradient pressure. Prior work has observed that VLA fine-tuning degrades inherited visual representations [14, 15, 16] and proposed broad preservation objectives; the action-fiber

*Corresponding author: linhaihao24@mails.uca.ac.cn

framing sharpens this to the question of which visual structure to preserve after filtering out the action-predictive component.

We introduce FIBERTUNE, a training-time residual preservation objective for VLA fine-tuning. FIBERTUNE first estimates action-predictive feature directions using an online action probe. It then applies the complementary feature-space filter to token representations, yielding a probe-filtered residual. A frozen visual teacher supplies a training-time reference for the residual visual structure; FIBERTUNE aligns centered, normalized residual token directions to the teacher and adds an effective-rank residual prior to prevent the residual from collapsing into a small number of teacher-correlated directions. At deployment, the policy is unchanged: the teacher, probe, and auxiliary adapter are removed.

Holding initialization, data, budget, and evaluator fixed, FIBERTUNE improves over task-loss-only fine-tuning in every one of six controlled simulation settings and on physical SO-101. On the CALVIN ABC→D chain evaluator, FIBERTUNE raises a $\pi_{0.5}$ task-loss baseline from 3.837 to 4.116 average subtasks and improves SR from 61.4% to 72.1%. On LIBERO, gains hold from both general and adapted checkpoints and transfer to an independent OpenVLA-OFT fine-tuning stack. On physical SO-101 pick-place, FIBERTUNE improves task success from 72.7% to 78.1%, with the largest gain on the held-out green block condition. Representation diagnostics show increased residual teacher alignment and effective rank, while full-token alignment can raise aggregate teacher similarity without strengthening residual structure.

Our contributions are:

- We formulate residual visual collapse in VLA fine-tuning through local action fibers, clarifying why action-supervised losses can discard visually meaningful but action-equivalent factors.
- We propose FIBERTUNE, an inference-free training-time objective that uses action-probe filtering to apply teacher alignment only to residual visual tokens, together with an effective-rank residual prior.
- We demonstrate consistent gains over task-loss-only fine-tuning across CALVIN, LIBERO ($\pi_{0.5}$ and OpenVLA-OFT), and physical SO-101, under fixed training conditions, and connect the gains to residual representation diagnostics.

2 Related Work

Vision-language-action policies. Robot foundation models increasingly combine pretrained vision and language representations with action decoders for manipulation and embodied control. Earlier systems grounded language in affordance scoring, zero-shot imitation, multimodal prompting, and embodied multimodal models [1, 2, 3, 4]. RT-1 and RT-2 demonstrated large-scale real-world robot policies and web-knowledge transfer to actions [5, 6]. RoboFlamingo, OpenVLA, and OpenVLA-OFT adapt pretrained vision-language models into robot policies and practical fine-tuning recipes [7, 8, 9], while Octo, CogACT, and π_0 -family policies explore generalist policy learning with different VLA training designs [10, 11, 12, 13]. Recent work also studies reinforced fine-tuning and long-horizon VLA execution [17, 18, 19]. FIBERTUNE is a training-time regularizer: it acts on intermediate visual-token representations during fine-tuning and introduces no additional parameters, modules, or inference-time overhead.

Action-supervised policy learning. Strong robot policies often reduce adaptation to supervised prediction of continuous actions, action chunks, or denoising targets. ACT and Diffusion Policy established high-performing action-sequence and diffusion-based visuomotor imitation recipes [20, 21]. Recent VLA recipes extend this pattern with faster parallel decoding and action tokenization [9, 22]. These objectives provide direct behavioral supervision but do not specify how much non-action visual structure should remain in intermediate representations, motivating the residual-preservation question studied here.

Representation preservation in VLA fine-tuning. Several recent papers identify representation degradation as a bottleneck for VLA adaptation. BlindVLA introduced a frozen-teacher visual alignment protocol that maps VLA visual tokens through a lightweight fixed adapter and aligns them to teacher patch features with a cosine loss [14]. MAPS preserves vision-language representations through module-wise proximity scheduling [16]. Spatial Forcing aligns VLA features to spatial foundation representations [23]. RS-CL uses robot-state-aware contrastive regularization to shape control-relevant representations [24]. These methods motivate representation preservation; their objectives generally operate on full representations, teacher spaces, state metrics, or architectural constraints. FIBERTUNE adopts the frozen-teacher/fixed-adapter alignment protocol from this line of work, but changes the aligned object: the teacher signal is applied after filtering action-predictive directions, and the residual is regularized by an effective-rank prior.

Information and anti-collapse principles. Our objective uses conditional information preservation as its design principle and implements it through trainable residual surrogates of the ideal mutual-information objective. This places FIBERTUNE near information bottleneck views [25, 26], LangForce’s language/action conditional-information analysis of shortcut behavior [27], and representation-rank diagnostics [28]. The effective-rank prior follows the same broad anti-collapse tradition as variance/covariance regularization in self-supervised learning [29, 30], but it is applied to action-filtered residual directions rather than generic image representations. We quantify these representation-geometry properties using CKA [31] to measure alignment between spaces and effective rank [28] to track covariance spread.

3 Method

FIBERTUNE targets the part of the visual-token representation that is weakly constrained by action supervision. We first identify this residual under a local action-fiber view, then describe the trainable probe-filtered residual used during fine-tuning. Below we state the trainable objective; the appendices collect the projector derivation, probe estimator, and implementation protocol.

3.1 Action fibers and residual visual collapse

Let V , L , and A denote the visual observation, language instruction, and supervised action target. For a sample (v, ℓ, a) , consider an intermediate visual-token representation $R_\theta(v, \ell) = [r_1, \dots, r_{T_v}] \in \mathbb{R}^{T_v \times d}$. A local prediction map h_θ maps these tokens to the supervised action target, and the task loss penalizes prediction errors through $\mathcal{L}_{\text{task}}$. For a fixed local target value, the corresponding action fiber is the level set of representations that induce the same supervised action target under the current policy head. Linearizing the local prediction map around the pooled visual feature $\bar{R}_\theta = T_v^{-1} \sum_t r_t$ gives

$$h_\theta(R_\theta + \Delta R) \approx h_\theta(R_\theta) + J_\theta \Delta \bar{r}, \quad (1)$$

where $\Delta \bar{r} = T_v^{-1} \sum_t \Delta r_t$ and J_θ is the Jacobian of the supervised action target with respect to \bar{R}_θ . Directions in $\text{Row}(J_\theta)$ change the supervised action target to first order and are directly constrained by the task loss. Under this pooled feature-axis linearization, directions in $\text{Null}(J_\theta)$ are tangent to the action fiber to first order: they produce no first-order change in the supervised action target, and therefore incur no first-order task-loss change. We denote by U_θ the feature-axis projection of R_θ onto $\text{Null}(J_\theta)$. Visual factors such as object identity, color, distractors, or future-relevant state can reside in U_θ and can be compressed during fine-tuning without a first-order penalty from the local action target.

Let τ be a frozen visual teacher, let $Z = \tau(V)$ be its visual-token representation, and let Z_c denote its token-centered form. The teacher is introduced as a training-time reference that makes residual visual preservation optimizable from the action dataset. FIBERTUNE uses the following conditional information objective as a preservation principle:

$$\max_{\theta} I(U_\theta; Z_c \mid A, L) \quad \text{s.t.} \quad \mathcal{L}_{\text{task}}(\theta) \leq \epsilon, \quad (2)$$

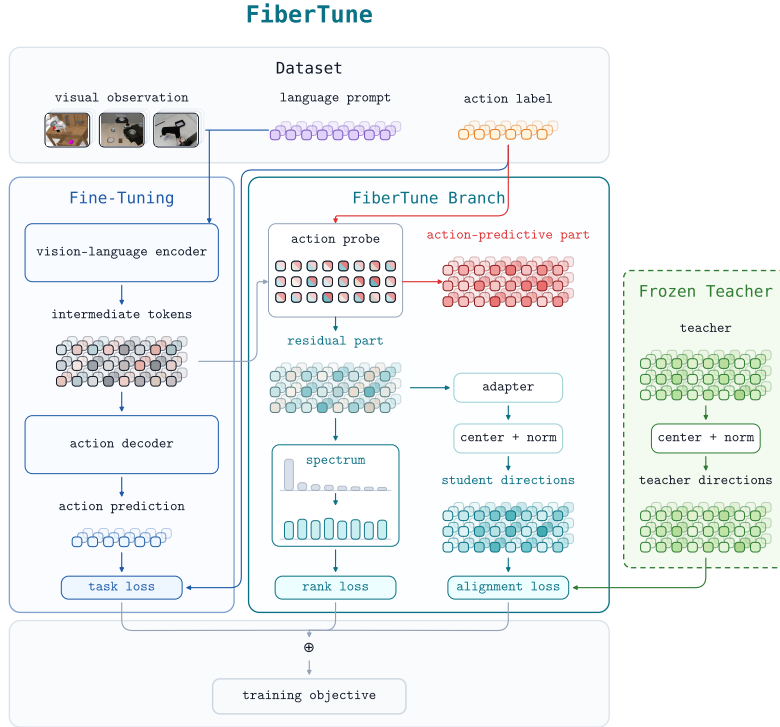


Figure 1: **FIBERTUNE overview.** Standard VLA fine-tuning does not supervise the action-orthogonal residual, allowing generalizable visual structure to collapse during adaptation. FIBERTUNE adds two training-time objectives—probe-filtered alignment to a frozen teacher and an effective-rank prior on the filtered residual—to preserve this structure; the teacher, probe, and auxiliary losses are removed at deployment.

Expanding by the chain rule gives

$$I(U_\theta; Z_c | A, L) = H(U_\theta | A, L) - H(U_\theta | Z_c, A, L), \quad (3)$$

which identifies two complementary pressures. The first term, $H(U_\theta | A, L)$, is the conditional entropy of the residual: maximizing it encourages the residual to span a high-rank subspace rather than collapsing onto a few dominant directions. The second term, $H(U_\theta | Z_c, A, L)$, is the residual uncertainty unexplained by the teacher: minimizing it encourages the residual to be predictable from teacher visual structure, i.e., to preserve the visual content the teacher encodes.

3.2 From ideal residuals to a computable probe-filtered residual

Computing U_θ exactly requires the local Jacobian of a large nonlinear VLA policy throughout fine-tuning, which is impractical. FIBERTUNE instead uses a scalable probe approximation to the same first-order geometry. The approximation estimates which feature directions are locally predictive of the supervised action target and removes those directions from the token representation. Concretely, FIBERTUNE fits a lightweight linear action probe from stop-gradient pooled visual-token features to the local supervised continuous action vector. The probe row space estimates the local action-predictive feature directions. Writing the resulting feature filter as P_{probe} , FIBERTUNE applies the complementary filter to the same visual-token set:

$$R_{\text{pf}} = R_\theta(I - P_{\text{probe}}). \quad (4)$$

Here R_{pf} is a scalable approximation to U_θ , with $R_\theta P_{\text{probe}}$ being the action-predictive component removed by the filter. During the policy update, P_{probe} is treated as a fixed filter: auxiliary gradients

flow through R_{pf} to R_{θ} , while the probe is updated only via its own action-regression objective. Because the probe is trained on pooled visual-token features, P_{probe} acts as shared feature-channel directions across all visual-token positions, consistent with the channel-wise structure of transformer hidden states.

3.3 Teacher-conditioned residual alignment

With R_{pf} in hand, we address the second pressure from Eq. (3): direct action supervision provides no target for action-preserving visual variation, so FIBERTUNE uses a frozen visual teacher as a training-time reference for residual visual structure. Like BlindVLA [14], we use a frozen teacher and a fixed randomly initialized per-token MLP adapter g ; unlike BlindVLA, we apply the loss to the probe-filtered residual R_{pf} rather than the full hidden state, and we center both representations along the token axis via $C_T = I_{T_v} - T_v^{-1}\mathbf{1}\mathbf{1}^\top$ before normalization so that cosine similarity acts on token-relative structure rather than the shared mean direction. The loss is computed on matched image-token spans: index t ranges over paired student and teacher visual tokens from the corresponding image view; language and action tokens are excluded. Let $Y_{\theta} = \text{norm}(C_T g(R_{\text{pf}}))$ and $\tilde{Z} = \text{norm}(Z_c)$; the alignment loss is

$$\mathcal{L}_{\text{align}} = -\mathbb{E}_t \left[\cos(Y_{\theta,t}, \tilde{Z}_t) \right]. \quad (5)$$

3.4 Effective-rank residual prior

The first pressure from Eq. (3) requires maximizing $H(U_{\theta} | A, L)$: spreading residual energy across directions rather than concentrating it. Alignment alone does not guarantee this; it can satisfy the teacher objective by concentrating teacher-correlated information onto a few dominant directions. Following covariance-spread anti-collapse objectives and rank diagnostics for learned representations [29, 30, 28], we therefore regularize the shape of the batch-token residual covariance. For covariance eigenvalues $\{\lambda_i\}_{i=1}^K$ of the probe-filtered residual samples in the VLA feature space before applying g , where K is the number of eigenvalues in the empirical spectrum, let $p_i = \lambda_i / \sum_j \lambda_j$ and $H_{\text{shape}}(R_{\text{pf}}) = -(\sum_i p_i \log p_i) / \log K$. We set $\mathcal{L}_{\text{rank}} = -H_{\text{shape}}(R_{\text{pf}})$, encouraging residual energy to occupy multiple directions. The final training objective is

$$\mathcal{L} = \mathcal{L}_{\text{task}} + \lambda_{\text{align}} \mathcal{L}_{\text{align}} + \lambda_{\text{rank}} \mathcal{L}_{\text{rank}}. \quad (6)$$

4 Experiments

4.1 Experimental setup

A task configuration is defined by its benchmark/task, policy, and initialization. Within each configuration, Baseline and FIBERTUNE share the training data, optimization budget, evaluator, and model-selection rule.

Benchmarks and metrics. We evaluate on two simulation benchmarks. CALVIN ABC→D evaluates multi-step language-conditioned manipulation with average completed subtasks and success at sequence lengths 1–5 using a chain evaluator over 1000 trials [32]. LIBERO evaluates standard manipulation suites with a four-suite protocol, using 10 tasks and 50 episodes per suite [33].

Policies and initializations. We evaluate $\pi_{0.5}$ policies on CALVIN and LIBERO using OpenPI-family source policies [13]; fine-tuning and LIBERO evaluation use the LeRobot stack [34], while CALVIN evaluation uses the RLinf chain-evaluation bridge [35, 36]. We evaluate OpenVLA-OFT policies on LIBERO using the original LIBERO environment [9]. For both backbones, we include general and adapted starting checkpoints to test first adaptation and continued specialization separately.

Table 1: **Main results under controlled fine-tuning.** FIBERTUNE outperforms the task-loss baseline in all six settings. Behavior values are primary single-seed runs (per-family default seed); the supplementary reports multi-seed averages and Wilson 95% confidence intervals.

Benchmark / task	Policy	Initialization	Metric	Baseline	FIBERTUNE	Gain
CALVIN ABC→D	$\pi_{0.5}$	general checkpoint	Avg. seq. len.	0.796	1.012	+0.216
CALVIN ABC→D	$\pi_{0.5}$	general checkpoint	SR (5) (%)	0.4	1.3	+0.9
CALVIN ABC→D	$\pi_{0.5}$	adapted checkpoint	Avg. seq. len.	3.837	4.116	+0.279
CALVIN ABC→D	$\pi_{0.5}$	adapted checkpoint	SR (5) (%)	61.4	72.1	+10.7
LIBERO	$\pi_{0.5}$	general checkpoint	SR (%)	92.35	93.35	+1.00
LIBERO	$\pi_{0.5}$	adapted checkpoint	SR (%)	95.75	97.10	+1.35
LIBERO	OpenVLA-OFT	general checkpoint	SR (%)	42.50	48.95	+6.45
LIBERO	OpenVLA-OFT	adapted checkpoint	SR (%)	95.35	96.15	+0.80

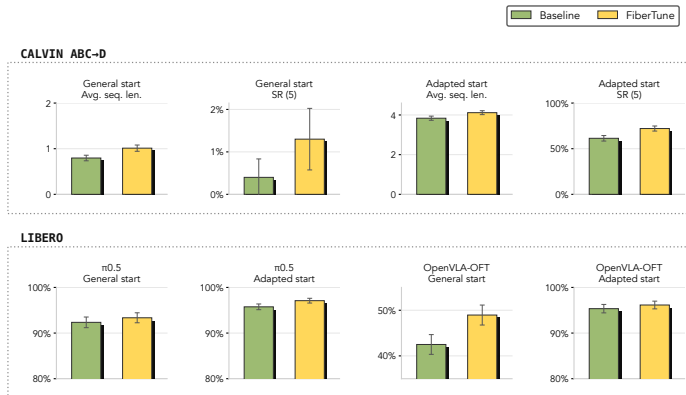


Figure 2: **Behavior improvements under controlled fine-tuning protocols.** FIBERTUNE consistently outperforms the task-loss baseline across all benchmarks and policies.

Baselines and controlled training protocol. Each comparison fixes the benchmark/task, policy, initialization, training data, budget, evaluator, and model-selection rule; within this protocol, the task-loss baseline and FIBERTUNE differ only in their fine-tuning objective. FIBERTUNE-specific choices — residual layer, teacher-token span, and auxiliary loss scales — are set per backbone before any result is collected and held constant across all rows for that backbone. Full protocol details are in the appendices.

4.2 Benchmark fine-tuning results

Table 1 reports the primary behavior results, organized by task configuration; further details are in the appendices.

CALVIN long-horizon chain evaluation. FIBERTUNE improves average sequence length from 3.837 to 4.116 and SR(5) from 61.4% to 72.1%. From a general (pre-CALVIN) $\pi_{0.5}$ checkpoint, both methods remain far from task completion under the fixed budget (SR(5) 0.4% vs 1.3%); we report this setting for completeness rather than as a primary result.

LIBERO standard benchmark. FIBERTUNE improves $\pi_{0.5}$ success from 92.35% to 93.35% from a general checkpoint and from 95.75% to 97.10% from an adapted checkpoint. Gains across both benchmarks confirm that FIBERTUNE is effective under different task distributions and evaluation environments.

Cross-architecture OpenVLA-OFT transfer. FIBERTUNE also transfers to a different architecture: it improves OpenVLA-OFT LIBERO success from 42.50% to 48.95% from a general OpenVLA checkpoint and from 95.35% to 96.15% from an adapted OpenVLA-OFT policy, showing that the gains hold across policy architectures and fine-tuning stages.

4.3 Real-world SO-101 pick-place

On the physical SO-101 pick-place task, under the same controlled protocol, FIBERTUNE improves task success from 72.7% to 78.1% over 128 trials spanning three in-distribution block colors and one held-out green condition. ID-color success improves from 81.2% to 83.3%; the held-out green condition improves from 46.9% to 62.5%. On the held-out green condition the gain is largest in magnitude (46.9%→62.5%); given the small per-condition sample ($n = 32$), we treat this as suggestive physical-robot evidence for improved color generalization, with the inference-time policy unchanged.

Table 2: **SO-101 physical pick-place results.** FIBERTUNE improves success rates across all stages and block colors, including the held-out OOD green block.

Stage / Condition	Baseline	FIBERTUNE	Gain
<i>Physical stage breakdown</i>			
Contact	120/128 (93.8%)	124/128 (96.9%)	+3.1
Lift	104/128 (81.2%)	106/128 (82.8%)	+1.6
Task success	93/128 (72.7%)	100/128 (78.1%)	+5.5
<i>Task success by color</i>			
ID colors	78/96 (81.2%)	80/96 (83.3%)	+2.1
OOD green	15/32 (46.9%)	20/32 (62.5%)	+15.6

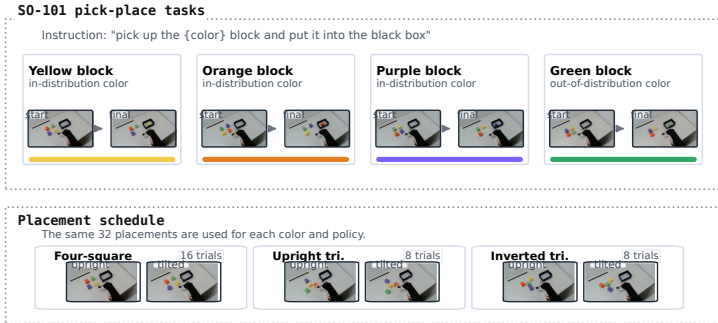


Figure 3: **Real-world SO-101 evaluation protocol.** The green block is the held-out OOD color; all other conditions are in-distribution.

4.4 Representation diagnostics

The central diagnostic question is whether FIBERTUNE changes the probe-filtered residual in ways that are visible beyond aggregate success rates. Table 3 reports the available representation diagnostics for the matched behavior comparisons. We use linear CKA and participation-ratio effective rank as established representation-similarity and covariance-spread diagnostics [31, 28]. Across all settings, FIBERTUNE increases both residual teacher CKA and residual effective rank. These diagnostics use metrics distinct from the training losses — effective rank is a participation ratio rather than the optimized spectral-entropy prior, and CKA is measured on the probe-filtered residual before the adapter g rather than on the post- g alignment target — so their consistent increase is representation-level evidence that FIBERTUNE preserves higher-rank, teacher-correlated residual structure, in line with the action-fiber motivation. Further diagnostics are in the appendices.

Table 3: **Representation diagnostics for controlled comparisons.** FIBERTUNE increases both metrics in every setting.

Evaluation setting	Method	Behavior	Residual CKA	Residual eff. rank
CALVIN / $\pi_{0.5}$ / general	Baseline	0.796	0.112	4.24
CALVIN / $\pi_{0.5}$ / general	FIBERTUNE	1.012	0.481	76.61
CALVIN / $\pi_{0.5}$ / adapted	Baseline	3.837	0.202	8.35
CALVIN / $\pi_{0.5}$ / adapted	FIBERTUNE	4.116	0.467	58.84
LIBERO / $\pi_{0.5}$ / general	Baseline	92.35	0.154	6.94
LIBERO / $\pi_{0.5}$ / general	FIBERTUNE	93.35	0.680	78.30
LIBERO / $\pi_{0.5}$ / adapted	Baseline	95.75	0.194	6.37
LIBERO / $\pi_{0.5}$ / adapted	FIBERTUNE	97.10	0.414	44.88
LIBERO / OpenVLA-OFT / general	Baseline	42.50	0.380	39.89
LIBERO / OpenVLA-OFT / general	FIBERTUNE	48.95	0.717	52.26
LIBERO / OpenVLA-OFT / adapted	Baseline	95.35	0.349	35.42
LIBERO / OpenVLA-OFT / adapted	FIBERTUNE	96.15	0.670	48.79

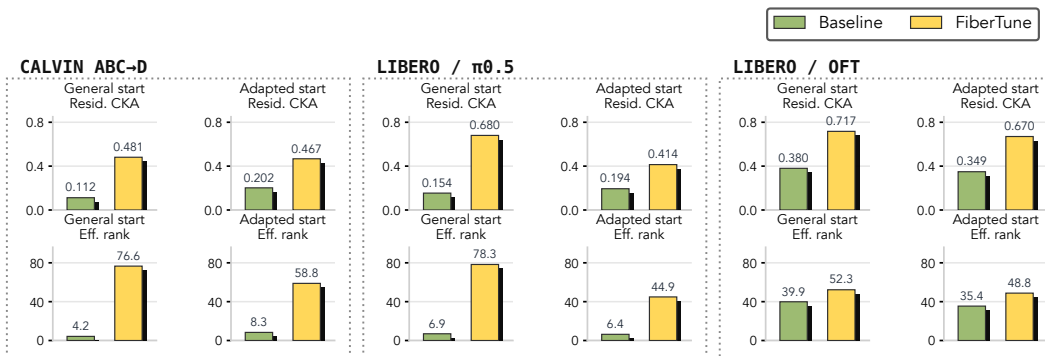


Figure 4: **Residual geometry diagnostics across six controlled settings.** FIBERTUNE increases residual CKA and effective rank in all six settings.

4.5 Component ablations

The ablations in Table 4 separate the source of the CALVIN gain. Full-token teacher alignment falls below the task-loss baseline, suggesting that, under matched loss weights, full-token alignment is not beneficial here whereas filtering action-predictive directions before alignment helps. The effective-rank prior alone recovers most of the gain, making it the dominant single component; residual alignment adds an incremental benefit, and the combination gives the best average sequence length and SR(5). Together, the ablations support the action-fiber motivation: maintaining spread in the action-orthogonal residual subspace is a primary source of the gain.

Table 4: **Component ablation on CALVIN.** The effective-rank prior is the dominant single component; filtering action-predictive directions before alignment is necessary, and the combination achieves the best result.

Variant	Teacher signal	Rank prior	Avg. seq.	SR(5)%
Baseline	none	no	3.837	61.4
Full-token align.	full tokens	no	3.685	58.3
Full-token + rank	full tokens	yes	3.956	65.6
Residual align.	pf-residual	no	3.980	66.2
Residual rank only	none	yes	4.064	70.5
FIBERTUNE	pf-residual	yes	4.116	72.1

5 Conclusion

Action-supervised fine-tuning constrains directions that cross action fibers but leaves fiber-tangent visual structure — where action-equivalent factors such as object color, category, and future-relevant state reside — without direct gradient pressure. FIBERTUNE addresses this by filtering action-predictive directions before applying teacher alignment and by maintaining the effective rank of the residual, both at training time only. Across CALVIN, LIBERO, and physical SO-101, FIBERTUNE consistently outperforms task-loss-only fine-tuning; representation diagnostics and com-

ponent ablations connect the gains to residual spread maintenance rather than teacher supervision alone. Explicitly regularizing the action-orthogonal residual subspace is a lightweight complement to standard task-loss fine-tuning with meaningful impact on behavioral generalization.

Limitations

FIBERTUNE introduces some training-time overhead: a frozen teacher, an online probe, and auxiliary losses are required during fine-tuning, although inference remains unchanged. The probe-filtered residual is a first-order, pooled-feature approximation to the local action-fiber residual; in settings where action prediction is highly nonlinear or where visual token positions contribute heterogeneously to the action target, the approximation may break down. We use benchmark-specific fixed auxiliary-to-task loss scales selected from short calibration runs; these scales are not automatically transferred across benchmarks, and broader automatic balancing is left for future work. Finally, physical-robot evidence is limited to a single task and manipulator; failure modes under more diverse real-world conditions remain uncharacterized and will require future investigation.

Acknowledgments

This work was supported in part by the Regional Innovation and Development Joint Fund of the National Natural Science Foundation of China under Grant U24A6005.

References

- [1] M. Ahn, A. Brohan, N. Brown, Y. Chebotar, O. Cortes, B. David, C. Finn, C. Fu, K. Gopalakrishnan, K. Hausman, et al. Do as i can, not as i say: Grounding language in robotic affordances. *arXiv preprint arXiv:2204.01691*, 2022.
- [2] E. Jang, A. Irpan, M. Khansari, D. Kappler, F. Ebert, C. Lynch, S. Levine, and C. Finn. Bc-z: Zero-shot task generalization with robotic imitation learning. In *Conference on Robot Learning*, pages 991–1002. PMLR, 2022.
- [3] Y. Jiang, A. Gupta, Z. Zhang, G. Wang, Y. Dou, Y. Chen, L. Fei-Fei, A. Anandkumar, Y. Zhu, and L. Fan. VIMA: Robot manipulation with multimodal prompts. In *International Conference on Machine Learning*, pages 14975–15022, 2023.
- [4] D. Driess, F. Xia, M. S. M. Sajjadi, C. Lynch, A. Chowdhery, B. Ichter, A. Wahid, J. Tompson, Q. Vuong, T. Yu, et al. Palm-e: An embodied multimodal language model. In *International Conference on Machine Learning*, pages 8469–8488, 2023.
- [5] A. Brohan, N. Brown, J. Carbajal, Y. Chebotar, J. Dabis, C. Finn, K. Gopalakrishnan, K. Hausman, A. Herzog, J. Hsu, et al. Rt-1: Robotics transformer for real-world control at scale. In *Robotics: Science and Systems*, 2023. doi:10.15607/rss.2023.xix.025.
- [6] A. Brohan, N. Brown, J. Carbajal, Y. Chebotar, X. Chen, K. Choromanski, T. Ding, D. Driess, A. Dubey, C. Finn, et al. RT-2: Vision-language-action models transfer web knowledge to robotic control. In *Proceedings of the Conference on Robot Learning*, 2023.
- [7] X. Li, M. Liu, H. Zhang, C. Yu, J. Xu, H. Wu, C. Cheang, Y. Jing, W. Zhang, H. Liu, et al. Vision-language foundation models as effective robot imitators. In *International Conference on Learning Representations*, 2024.
- [8] M. J. Kim, K. Pertsch, S. Karamcheti, T. Xiao, A. Balakrishna, S. Nair, R. Rafailov, E. Foster, G. Lam, P. Sanketi, Q. Vuong, T. Kollar, B. Burchfiel, R. Tedrake, D. Sadigh, S. Levine, P. Liang, and C. Finn. Openvla: An open-source vision-language-action model. In *Proceedings of the Conference on Robot Learning*, 2024.
- [9] M. J. Kim, C. Finn, and P. Liang. Fine-tuning vision-language-action models: Optimizing speed and success. *arXiv preprint arXiv:2502.19645*, 2025.
- [10] Octo Model Team, D. Ghosh, H. Walke, K. Pertsch, K. Black, O. Mees, S. Dasari, J. Hejna, C. Xu, T. Kreiman, Y. L. Tan, L. Y. Chen, P. Sanketi, Q. Vuong, T. Xiao, D. Sadigh, C. Finn, and S. Levine. Octo: An open-source generalist robot policy. In *Robotics: Science and Systems*, 2024.
- [11] Q. Li, Y. Liang, Z. Wang, L. Luo, X. Chen, M. Liao, F. Wei, Y. Deng, S. Xu, Y. Zhang, et al. CogACT: A foundational vision-language-action model for synergizing cognition and action in robotic manipulation. *arXiv preprint arXiv:2411.19650*, 2024.
- [12] K. Black, N. Brown, D. Driess, A. Esmail, M. Equi, C. Finn, N. Fusai, L. Groom, K. Hausman, B. Ichter, S. Jakubczak, T. Jones, L. Ke, S. Levine, A. Li-Bell, M. Mothukuri, S. Nair, K. Pertsch, L. X. Shi, J. Tanner, Q. Vuong, A. Walling, H. Wang, and U. Zhilinsky. π_0 : A vision-language-action flow model for general robot control. *arXiv preprint arXiv:2410.24164*, 2024.
- [13] Physical Intelligence, K. Black, N. Brown, J. Darpinian, K. Dhabalia, D. Driess, A. Esmail, M. Equi, C. Finn, N. Fusai, M. Y. Galliker, D. Ghosh, L. Groom, K. Hausman, B. Ichter, S. Jakubczak, T. Jones, L. Ke, D. LeBlanc, S. Levine, A. Li-Bell, M. Mothukuri, S. Nair, K. Pertsch, A. Z. Ren, L. X. Shi, L. Smith, J. T. Springenberg, K. Stachowicz, J. Tanner, Q. Vuong, H. Walke, A. Walling, H. Wang, L. Yu, and U. Zhilinsky. $\pi_{0.5}$: A vision-language-action model with open-world generalization. *arXiv preprint arXiv:2504.16054*, 2025.

- [14] N. Kachaev, M. Kolosov, D. Zelezetsky, A. K. Kovalev, and A. I. Panov. Don't blind your vla: Aligning visual representations for ood generalization. *arXiv preprint arXiv:2510.25616*, 2025.
- [15] Z. Zhang, X.-H. Chen, Y. Wang, Y. Sun, W. Luo, H. Ren, H. Lin, and Y. Yu. On the representation degradation in vision-language-action models. *OpenReview*, 2025.
- [16] C. Huang, M. M. Zhang, R. Azarcon, G. Chou, and Z. Kira. Maps: Preserving vision-language representations via module-wise proximity scheduling for better vision-language-action generalization. *arXiv preprint arXiv:2511.19878*, 2025.
- [17] Y. Chen, S. Tian, S. Liu, Y. Zhou, H. Li, and D. Zhao. Conrft: A reinforced fine-tuning method for vla models via consistency policy. *arXiv preprint arXiv:2502.05450*, 2025.
- [18] D. Huang, Z. Fang, T. Zhang, Y. Li, L. Zhao, and C. Xia. Co-rft: Efficient fine-tuning of vision-language-action models through chunked offline reinforcement learning. *arXiv preprint arXiv:2508.02219*, 2025.
- [19] Y. Fan, P. Ding, S. Bai, X. Tong, Y. Zhu, H. Lu, F. Dai, W. Zhao, Y. Liu, S. Huang, Z. Fan, B. Chen, and D. Wang. Long-vla: Unleashing long-horizon capability of vision language action model for robot manipulation. *arXiv preprint arXiv:2508.19958*, 2025.
- [20] T. Z. Zhao, V. Kumar, S. Levine, and C. Finn. Learning fine-grained bimanual manipulation with low-cost hardware. In *Robotics: Science and Systems*, 2023. doi:10.15607/rss.2023.xix.016.
- [21] C. Chi, S. Feng, Y. Du, Z. Xu, E. Cousineau, B. Burchfiel, and S. Song. Diffusion policy: Visuomotor policy learning via action diffusion. In *Robotics: Science and Systems*, 2023.
- [22] K. Pertsch, K. Stachowicz, B. Ichter, D. Driess, S. Nair, Q. Vuong, O. Mees, C. Finn, and S. Levine. FAST: Efficient action tokenization for vision-language-action models. *arXiv preprint arXiv:2501.09747*, 2025.
- [23] F. Li, W. Song, H. Zhao, J. Wang, P. Ding, D. Wang, L. Zeng, and H. Li. Spatial forcing: Implicit spatial representation alignment for vision-language-action model. *arXiv preprint arXiv:2510.12276*, 2025.
- [24] T. Kim, J. Lee, M. Koo, D. Kim, K. Lee, C. Kim, Y. Seo, and J. Shin. Contrastive representation regularization for vision-language-action models. *arXiv preprint arXiv:2510.01711*, 2025.
- [25] N. Tishby, F. C. Pereira, and W. Bialek. The information bottleneck method. In *Proceedings of the 37th Annual Allerton Conference on Communication, Control, and Computing*, 1999.
- [26] S. Bai, W. Zhou, P. Ding, W. Zhao, D. Wang, and B. Chen. Rethinking latent redundancy in behavior cloning: An information bottleneck approach for robot manipulation. *arXiv preprint arXiv:2502.02853*, 2025.
- [27] S. Lian, B. Yu, X. Lin, L. T. Yang, Z. Shen, C. Wu, Y. Miao, C. Huang, and K. Chen. Langforce: Bayesian decomposition of vision language action models via latent action queries. *arXiv preprint arXiv:2601.15197*, 2026.
- [28] Q. Garrido, R. Balestriero, L. Najman, and Y. LeCun. Rankme: Assessing the downstream performance of pretrained self-supervised representations by their rank. In *International Conference on Machine Learning*, pages 10929–10974, 2023.
- [29] A. Bardes, J. Ponce, and Y. LeCun. Vicreg: Variance-invariance-covariance regularization for self-supervised learning. In *International Conference on Learning Representations*, 2022.
- [30] J. Zbontar, L. Jing, I. Misra, Y. LeCun, and S. Deny. Barlow twins: Self-supervised learning via redundancy reduction. In *International Conference on Machine Learning*, 2021.

- [31] S. Kornblith, M. Norouzi, H. Lee, and G. Hinton. Similarity of neural network representations revisited. In *International Conference on Machine Learning*, 2019.
- [32] O. Mees, L. Hermann, E. Rosete-Beas, and W. Burgard. Calvin: A benchmark for language-conditioned policy learning for long-horizon robot manipulation tasks. *IEEE Robotics and Automation Letters*, 7(3):7327–7334, 2022.
- [33] B. Liu, Y. Zhu, C. Gao, Y. Feng, Q. Liu, Y. Zhu, and P. Stone. Libero: Benchmarking knowledge transfer for lifelong robot learning. In *Advances in Neural Information Processing Systems*, 2023.
- [34] R. Cadene, S. Alibert, F. Capuano, M. Aractingi, A. Zouitine, P. Kooijmans, J. Choghari, M. Russi, C. Pascal, S. Palma, D. Aubakirova, M. Shukor, J. Moss, A. Soare, Q. Lhoest, Q. Gallouédec, and T. Wolf. Lerobot: An open-source library for end-to-end robot learning. In *The Fourteenth International Conference on Learning Representations*, 2026. URL <https://arxiv.org/abs/2602.22818>.
- [35] C. Yu, Y. Wang, Z. Guo, H. Lin, S. Xu, H. Zang, Q. Zhang, Y. Wu, C. Zhu, J. Hu, et al. Rlinf: Flexible and efficient large-scale reinforcement learning via macro-to-micro flow transformation. *arXiv preprint arXiv:2509.15965*, 2025.
- [36] H. Zang, M. Wei, S. Xu, Y. Wu, Z. Guo, Y. Wang, H. Lin, P. Wang, L. Shi, Y. Xie, Z. Xu, et al. Rlinf-vla: A unified and efficient framework for reinforcement learning of vision-language-action models. *arXiv preprint arXiv:2510.06710*, 2025.
- [37] T. M. Cover and J. A. Thomas. *Elements of Information Theory*. Wiley-Interscience, 2 edition, 2006.
- [38] K. V. Mardia and P. E. Jupp. *Directional Statistics*. Wiley Series in Probability and Statistics. John Wiley & Sons, 1999. doi:10.1002/9780470316979.
- [39] G. Heinrich, M. Ranzinger, H. Yin, Y. Lu, J. Kautz, A. Tao, B. Catanzaro, and P. Molchanov. RADIOv2.5: Improved baselines for agglomerative vision foundation models. In *Proceedings of the IEEE/CVF Conference on Computer Vision and Pattern Recognition*, pages 22487–22497, 2025.
- [40] J. Bjorck, F. Castañeda, N. Cherniadev, X. Da, R. Ding, L. Fan, Y. Fang, D. Fox, F. Hu, S. Huang, et al. GR00T N1: An open foundation model for generalist humanoid robots. *arXiv preprint arXiv:2503.14734*, 2025.

A Technical details

A.1 From ideal orthogonal residuals to probe-filtered residuals

For a sample (v, ℓ, a) , FIBERTUNE operates on an intermediate visual-token representation

$$R_\theta(v, \ell) = [r_1, \dots, r_{T_v}] \in \mathbb{R}^{T_v \times d}, \quad (7)$$

and the local prediction map h_θ is trained with

$$\mathcal{L}_{\text{task}}(\theta) = \mathbb{E}[c_{\text{task}}(h_\theta(R_\theta), A)]. \quad (8)$$

For a fixed local action target a , the action fiber is the level set

$$\mathcal{F}_{a,\theta} = \{R : h_\theta(R) = a\}. \quad (9)$$

Let $Z = \tau(V)$ be the visual-token representation of the frozen teacher and let $Z_c = C_T Z$ be its token-centered form. The ideal preservation objective in the main paper uses the standard information-theoretic decomposition [37]

$$I(U_\theta; Z_c | A, L) = H(U_\theta | A, L) - H(U_\theta | Z_c, A, L), \quad (10)$$

which separates residual spread from teacher predictability.

We formalize the action-fiber residual with a first-order approximation of the supervised action map. Let $\bar{R}_\theta = T_v^{-1} \sum_t R_{\theta,t}$ be the pooled visual-token representation and let J_θ denote the Jacobian of the local action target with respect to the pooled feature \bar{R}_θ . Under the first-order geometry used in the main text, the ideal residual projector is

$$Q_\theta = I - J_\theta^\top (J_\theta J_\theta^\top)^\dagger J_\theta, \quad U_\theta = R_\theta Q_\theta. \quad (11)$$

The projector Q_θ keeps the component of R_θ in the first-order tangent space of the local action fiber. During training, FIBERTUNE uses a probe-defined feature filter in place of this Jacobian projector. The probe is fit from detached pooled visual-token features to the supervised action target,

$$W^* = \arg \min_W \mathbb{E} \|A - W \bar{R}_\theta\|^2, \quad (12)$$

uses its row space to form the ridge-stabilized feature filter

$$P_{\text{probe}} = W^{*\top} (W^* W^{*\top} + \eta I)^{-1} W^*, \quad (13)$$

and applies the complementary feature filter to the same visual-token set:

$$R_{\text{pf}} = R_\theta (I - P_{\text{probe}}). \quad (14)$$

The alignment loss and effective-rank prior both act on R_{pf} during training.

A.2 Directional alignment objective

The directional alignment term acts on the probe-filtered residual R_{pf} . The adapter g maps each residual token to teacher feature space; the centering matrix $C_T = I_{T_v} - T_v^{-1} \mathbf{1}\mathbf{1}^\top$ removes the token mean before row-wise normalization. The cosine term therefore compares token-relative residual structure. The resulting directions and alignment loss are

$$\begin{aligned} Y_\theta &= \text{norm}(C_T g(R_{\text{pf}})) \\ \tilde{Z} &= \text{norm}(Z_c) = \text{norm}(C_T Z) \\ \mathcal{L}_{\text{align}} &= -\mathbb{E}_t [\cos(Y_{\theta,t}, \tilde{Z}_t)]. \end{aligned} \quad (15)$$

A vMF-style directional likelihood over normalized residual directions gives the cosine form used in this objective [38]. For a fixed concentration $\kappa > 0$,

$$\log p(Y_{\theta,t} | \tilde{Z}_t, \kappa) = \kappa Y_{\theta,t}^\top \tilde{Z}_t + \text{const}(\kappa), \quad (16)$$

so maximizing the directional likelihood is equivalent to minimizing $-\cos(Y_{\theta,t}, \tilde{Z}_t)$. The alignment term is therefore a directional likelihood objective on the action-filtered residual.

A.3 Effective-rank prior

For the probe-filtered residual R_{pf} , the effective-rank prior uses the empirical covariance over batch-token residual samples in the VLA feature space before applying g . For a mini-batch \mathcal{B} and T_v selected token positions, the empirical spectrum contains K nonzero eigenvalues with $K \leq \min(|\mathcal{B}|T_v - 1, d)$. With trace-normalized eigenvalues p_i , the normalized score $-(\sum_i p_i \log p_i) / \log K$ is scale-free and penalizes concentration into a small number of residual directions. Concretely, for covariance eigenvalues $\{\lambda_i\}$,

$$\begin{aligned} p_i &= \frac{\lambda_i}{\sum_j \lambda_j} \\ H_{\text{shape}}(R_{\text{pf}}) &= -\frac{1}{\log K} \sum_i p_i \log p_i \\ \mathcal{L}_{\text{rank}} &= -H_{\text{shape}}(R_{\text{pf}}). \end{aligned} \tag{17}$$

The rank term therefore favors residual covariance spectra that remain spread across multiple directions.

A.4 Probe row-space consistency

The action probe estimates the local action-changing row space under a centered local linear model.

Proposition. Suppose the centered pooled representation and action target satisfy

$$\tilde{R} = \bar{R}_\theta - \mathbb{E}[\bar{R}_\theta], \quad \tilde{A} = A - \mathbb{E}[A], \tag{18}$$

and

$$\tilde{A} = J_0 \tilde{R} + \varepsilon, \quad \mathbb{E}[\varepsilon \mid \tilde{R}] = 0, \tag{19}$$

with $\mathbb{E}[\tilde{R}\tilde{R}^\top]$ full rank. Then the unregularized population least-squares probe

$$W_0^* = \arg \min_W \mathbb{E} \|\tilde{A} - W\tilde{R}\|^2 \tag{20}$$

recovers the local action-predictive row space.

Proof. The population solution is

$$\begin{aligned} W_0^* &= \mathbb{E}[\tilde{A}\tilde{R}^\top] \mathbb{E}[\tilde{R}\tilde{R}^\top]^{-1} \\ &= J_0 \mathbb{E}[\tilde{R}\tilde{R}^\top] \mathbb{E}[\tilde{R}\tilde{R}^\top]^{-1} = J_0. \end{aligned} \tag{21}$$

Thus the probe row space equals the row space of the local action map under the stated local model. With finite samples, ridge stabilization gives the filter P_{probe} used by FIBERTUNE.

Empirical limit. Let \widehat{W}_n be the ridge probe fitted from n detached pooled visual-token samples under the same local linear model. If the empirical cross-covariance and feature covariance converge to their population values, the feature covariance remains nonsingular, and the ridge coefficient $\eta_n \rightarrow 0$, then $\widehat{W}_n \rightarrow W_0^*$. Consequently, the empirical probe row space and the corresponding filter $P_{\text{probe}}(\widehat{W}_n)$ converge to the population first-order action-predictive row-space filter.

B Protocol details

B.1 Implementation stacks and seed conventions

Our experiments span two VLA model families whose public training and evaluation toolchains differ, so we record the implementation stack used in each setting. The $\pi_{0.5}$ family was released through Physical Intelligence/OpenPI [12, 13], but our $\pi_{0.5}$ fine-tuning uses the Hugging Face LeRobot stack [34]. Within every controlled comparison, the task-loss baseline and FIBERTUNE follow

the same LeRobot fine-tuning path and differ only in the residual-preservation losses that FIBER-TUNE adds. Evaluation depends on the benchmark. LIBERO uses the LeRobot evaluation stack, and SO-101 uses the LeRobot real-robot recording pipeline. For CALVIN, policies are first exported to the OpenPI checkpoint contract and scored by the RLinf/OpenPI chain evaluator [35, 36], so the baseline and FIBERTUNE stay under one long-horizon evaluator. The OpenVLA-OFT experiments instead use that family’s own OpenVLA-OFT codebase, data pipeline, and LIBERO evaluator [9].

The seeds used in our experiments are the public defaults of the corresponding implementation toolchains. OpenVLA-OFT uses seed 7 as the default LIBERO evaluation seed in its released evaluation script.¹ OpenPI uses seed 42 as the default training seed in its public training configuration,² and LeRobot uses seed 1000 as the default seed in its released training configuration³ and evaluation configuration.⁴

B.2 Controlled protocol summary

Each controlled comparison holds the starting checkpoint, training data, optimization budget, evaluator, and model-selection rule identical between the task-loss baseline and FIBERTUNE, so that any behavioral difference is attributable to the residual-preservation objective. Table B.1 records the initialization, training data, and evaluator for each comparison; checkpoint provenance is in Table B.2 and the optimization budget and schedule in Table B.4.

Table B.1: Controlled protocol details: initialization, training data, and evaluator fixed inside each controlled comparison.

Evaluation setting	Model	Initialization	Training data	Evaluator
CALVIN ABC→D	$\pi_{0.5}$	adapted	CALVIN ABC	1000 CALVIN chain-evaluation trials
CALVIN ABC→D	$\pi_{0.5}$	general	CALVIN ABC	1000 CALVIN chain-evaluation trials
LIBERO	$\pi_{0.5}$	general	LIBERO task suites	10 tasks and 50 episodes per suite
LIBERO	$\pi_{0.5}$	adapted	LIBERO task suites	10 tasks and 50 episodes per suite
LIBERO	OpenVLA-OFT	general	LIBERO task suites	10 tasks and 50 episodes per suite
LIBERO	OpenVLA-OFT	adapted	LIBERO task suites	10 tasks and 50 episodes per suite
SO-101 pick-place	$\pi_{0.5}$	real-world source	90 SO-101 demonstrations; yellow/orange/purple ID colors; green held out for OOD evaluation	128 physical trials per arm

CALVIN normalization and the chain-evaluation bridge use the released RLinf/OpenPI CALVIN asset.

B.3 Source-policy provenance

Table B.2 records the starting-policy provenance for the controlled comparisons in the main paper.

Table B.2: Starting-policy provenance for the controlled task configurations.

Task configuration	Training start	Source-policy provenance
CALVIN / $\pi_{0.5}$ / general	general checkpoint	lerobot/pi05_base.
CALVIN / $\pi_{0.5}$ / adapted	adapted checkpoint	RLinf/RLinf-Pi05-CALVIN-ABC-D-SFT.
LIBERO / $\pi_{0.5}$ / general	general checkpoint	lerobot/pi05_base.
LIBERO / $\pi_{0.5}$ / adapted	adapted checkpoint	lerobot/pi05_libero.
LIBERO / OpenVLA-OFT / general	general checkpoint	openvla/openvla-7b.
LIBERO / OpenVLA-OFT / adapted	adapted checkpoint	moojink/openvla-7b-offt- finetuned-libero-spatial-object-goal-10.
SO-101 / $\pi_{0.5}$	real-world source policy	Trained from lerobot/pi05_base on the 90-demonstration SO-101 source set.

¹https://raw.githubusercontent.com/moojink/openvla-offt/main/experiments/robot/libero/run_libero_eval.py

²<https://raw.githubusercontent.com/Physical-Intelligence/openpi/main/src/openpi/training/config.py>

³<https://raw.githubusercontent.com/huggingface/lerobot/main/src/lerobot/configs/train.py>

⁴<https://raw.githubusercontent.com/huggingface/lerobot/main/src/lerobot/configs/eval.py>

B.4 Implementation protocol for residual objectives

Table B.3 records the implementation choices behind FIBERTUNE’s residual objectives.

Table B.3: Implementation protocol for FIBERTUNE residual losses. Values summarize the controlled comparisons reported in the main paper; “Same” marks an OpenVLA-OFT setting identical to the $\pi_{0.5}$ column.

Field	$\pi_{0.5}$ experiments	OpenVLA-OFT experiments
Visual-token source	Prefix-tower image-token slice from an intermediate policy layer	VLA hidden-state image-token span from an intermediate policy layer
Layer used in reported runs	Prefix tower layer 8	Layer 16
Teacher	Frozen RADIO visual teacher, c-radio.v3-1 [39]	Same
Teacher-alignment protocol	Frozen-teacher, fixed-adapter token cosine alignment applied to R_{pf}	Same
Camera policy	Primary camera view	Same
Token pairing	Student image-token count is matched to teacher patch-token count for the selected view; mismatched tokenizations require an explicit adapter	Same
Probe target	Local first-step continuous action vector used for probe fitting	Same
Probe fitting	Online no-bias linear probe on detached pooled visual-token features; updated before projection	Same
Ridge filter	$P_{probe} = W^T(WW^T + \eta I)^{-1}W$, $\eta = 10^{-4}$	Same
Adapter g	Randomly initialized MLP adapter mapping each token position independently into teacher feature space; adapter hidden width 2048; frozen after initialization in reported experiments	Same
Auxiliary gradient path	Gradients pass through fixed P_{probe} and fixed g to the policy representation; probe and adapter g are not optimized by \mathcal{L}_{align}	Same
Covariance samples for eff.-rank prior	Batch-token samples from R_{pf} before applying g	Same

B.5 Hyperparameters

Table B.4: Compact hyperparameter summary for the controlled comparisons in the main paper.

Evaluation setting	Batch / accum. / GPUs	Budget	LR schedule	Aux coefficients
CALVIN / $\pi_{0.5}$ / general	8 / 4 / 1	6,000 steps	$2.5 \times 10^{-5} \rightarrow 2.5 \times 10^{-6}$ cosine; 1k warmup	0.0125 / 0.00625; 1k aux warmup; decay 3k–6k to 0.5
CALVIN / $\pi_{0.5}$ / adapted	8 / 4 / 1	6,000 steps	$2.5 \times 10^{-5} \rightarrow 2.5 \times 10^{-6}$ cosine; 1k warmup	0.0125 / 0.00625; 1k aux warmup; decay 3k–6k to 0.5
LIBERO / $\pi_{0.5}$ / general	8 / 4 / 2	6,000 steps	$5 \times 10^{-5} \rightarrow 5 \times 10^{-6}$ cosine; 1k warmup	0.0125 / 0.00625; 1k aux warmup; decay 3k–6k to 0.5
LIBERO / $\pi_{0.5}$ / adapted	8 / 4 / 1	6,000 steps	$2.5 \times 10^{-5} \rightarrow 2.5 \times 10^{-6}$ cosine; 1k warmup	0.0125 / 0.00625; 1k aux warmup; decay 3k–6k to 0.5
LIBERO / OpenVLA-OFT / general	8 / 1 / 1	20,000 steps	10^{-4} ; 1k warmup + constant	0.0125 / 0.00625; 1k aux warmup; decay 10k–20k to 0.5
LIBERO / OpenVLA-OFT / adapted	8 / 1 / 1	15,000 steps	10^{-4} ; 1k warmup + constant	0.0125 / 0.00625; 1k aux warmup; decay 10k–20k to 0.5
SO-101 / $\pi_{0.5}$ / pick-place policy	8 / 8 / 1	6,000 steps	$5 \times 10^{-5} \rightarrow 5 \times 10^{-6}$ cosine; 1k warmup	0.003125 / 0.0015625; 3k aux warmup; decay after 4.5k to 0.5

Batch denotes per-device batch size, and the optimizer effective batch is batch size \times accumulation \times GPU count. The residual probe and residual covariance estimators are computed on each forward micro-batch rather than over accumulated gradients. Reported runs used NVIDIA GPUs with at least 48GB of device memory; the GPU count for each comparison is listed in the table.

Auxiliary-coefficient selection. We choose the auxiliary coefficients from short calibration runs that keep the tail value of the weighted auxiliary pressure relative to the task loss,

$$\rho_{aux} = \frac{\lambda_{align}|\mathcal{L}_{align}| + \lambda_{rank}|\mathcal{L}_{rank}|}{\mathcal{L}_{task}}, \quad (22)$$

within an empirical range of approximately 3–6%.

B.6 Diagnostic definitions and probe-fitting protocol

The representation diagnostics reported in the main paper use a probe refit for analysis, separate from the online probe weights saved during training. The diagnostic target is the 7D per-step action vector. For CALVIN and $\pi_{0.5}$ LIBERO, the diagnostic probe is four-fold cross-fit; for OpenVLA-OFT, the exported diagnostics use an in-sample probe. In this protocol, R_{pf} denotes the residual formed by the refit diagnostic probe. Residual CKA is linear CKA between R_{pf} and the matched teacher features before the adapter g . Residual effective rank is the participation-ratio statistic $d_{\text{eff}} = (\sum_i \lambda_i)^2 / \sum_i \lambda_i^2$ computed from the residual covariance spectrum. The training objective uses the normalized spectral entropy H_{shape} from Appendix A.3; the reported effective rank is a complementary summary of the same covariance spectrum.

B.7 BlindVLA-style full-token alignment baseline

The main-paper “Full-token align.” ablation is our $\pi_{0.5}$ / LeRobot implementation of the BlindVLA-style frozen-teacher alignment protocol [14]. It uses the same frozen RADIO teacher, fixed randomly initialized per-token adapter, token centering, and cosine teacher-alignment loss as the FIBERTUNE alignment branch, but applies the teacher signal to the unfiltered intermediate token representation instead of to R_{pf} and does not fit or apply an action probe. This variant is therefore a controlled transfer of the BlindVLA-style full-token alignment objective into the $\pi_{0.5}$ training stack, with the same CALVIN starting checkpoint, data, budget, and evaluator as the other component ablations. It separates the effect of importing the full-token visual-alignment protocol from the effect of residualizing the aligned representation. The comparison also clarifies why the BlindVLA-style objective can be strong under the BlindVLA evaluation protocol while showing a different pattern in our matched CALVIN continuation. BlindVLA evaluates visual alignment in OOD-oriented settings, including Simpler-based generalization axes and the VL-Think suite, where low-level action complexity is bounded and success emphasizes grounding visual categories, concepts, and targets under distribution shift [14]. In that setting, preserving the full visual representation is closely aligned with the benchmark pressure. Our component ablation ports the same full-token pressure into a matched CALVIN fine-tuning setting, where success depends on preserving long-horizon task execution under the adapted policy. The comparison is therefore complementary: BlindVLA tests whether full-token visual preservation improves OOD grounding, while our controlled transfer exposes the trade-off that can arise when the same pressure is applied to a CALVIN continuation policy. A BlindVLA-style full-token implementation regularizes the complete intermediate representation; this is useful when the benchmark rewards broad visual-semantic retention, but it can also constrain directions that the adapted policy uses for in-distribution long-horizon execution. FIBERTUNE keeps the teacher-alignment protocol but first filters action-predictive directions, so the alignment pressure targets residual visual structure rather than the full task-conditioned representation. This residualization lets FIBERTUNE retain the visual-alignment signal while reducing its interference with the action-conditioned representation used by the policy.

C Additional analyses

C.1 CALVIN paired-seed material

Table C.5 reports paired CALVIN seeds for the adapted starting checkpoint as a robustness check, under the same 6k fixed-budget protocol as the main CALVIN adapted comparison.

C.2 LIBERO per-suite success rates

Table C.6 reports the per-suite success rates behind the aggregate LIBERO rows where suite-level exports are available. The $\pi_{0.5}$ / adapted block spans seeds 7, 42, and 1000, with a three-seed average gain of +0.70 percentage points. For the low-budget OpenVLA-OFT / general-start setting, the +6.45 pp aggregate gain is concentrated in the spatial and object suites, reflecting larger suite-level variation before convergence.

Table C.5: CALVIN paired-seed material for the adapted starting checkpoint. SR1–SR5 report the percentage of rollouts that complete at least 1–5 consecutive subtasks.

Seed	Method	Avg.	SR1	SR2	SR3	SR4	SR5
5	Baseline	3.682	90.7	81.1	73.1	65.6	57.7
	FIBERTUNE	4.044	93.0	85.9	80.2	75.2	70.1
6	Baseline	3.980	93.0	85.6	78.9	73.2	67.3
	FIBERTUNE	4.105	94.2	87.4	81.8	76.6	70.5
7	Baseline	3.837	93.2	84.7	75.9	68.5	61.4
	FIBERTUNE	4.116	94.3	87.3	80.9	77.0	72.1
Mean	Baseline	3.833	92.3	83.8	76.0	69.1	62.1
	FIBERTUNE	4.088	93.8	86.9	81.0	76.3	70.9

Table C.6: LIBERO per-suite success rates for available exports. Values are success rates in percent over 500 episodes per suite.

Setting	Seed	Method	Spatial	Object	Goal	LIBERO-10	Avg.
$\pi_{0.5}$ / general	7	Baseline	93.2	96.6	92.4	87.2	92.35
$\pi_{0.5}$ / general	7	FIBERTUNE	94.2	98.6	93.0	87.6	93.35
$\pi_{0.5}$ / adapted	1000	Baseline	96.4	98.0	95.6	93.0	95.75
$\pi_{0.5}$ / adapted	1000	FIBERTUNE	97.8	98.8	97.8	94.0	97.10
$\pi_{0.5}$ / adapted	7	Baseline	96.4	99.0	95.8	94.2	96.35
$\pi_{0.5}$ / adapted	7	FIBERTUNE	97.0	98.6	98.4	92.8	96.70
$\pi_{0.5}$ / adapted	42	Baseline	97.6	98.2	95.6	93.6	96.25
$\pi_{0.5}$ / adapted	42	FIBERTUNE	97.4	99.0	96.2	94.0	96.65
$\pi_{0.5}$ / adapted	Mean	Baseline	96.80	98.40	95.67	93.60	96.12
$\pi_{0.5}$ / adapted	Mean	FIBERTUNE	97.40	98.80	97.47	93.60	96.82
OpenVLA-OFT / general	7	Baseline	19.8	66.0	67.0	17.2	42.50
OpenVLA-OFT / general	7	FIBERTUNE	35.8	89.4	58.8	11.8	48.95

C.3 Confidence intervals for success metrics

Table C.7 reports Wilson 95% confidence intervals for the binomial success metrics in the main paper. For the CALVIN and LIBERO adapted settings we add a three-seed pooled interval alongside the primary single-seed run, with the per-seed numbers in Tables C.5 and C.6. LIBERO intervals pool the four task suites of each comparison. For SO-101, the all-colors rows pool all 128 physical trials per arm (including the held-out green condition), while the ID-colors row pools only the yellow, orange, and purple trials.

C.4 CALVIN low-learning-rate calibration point

Table C.8 reports a low-learning-rate CALVIN calibration point. It shares the adapted starting checkpoint, repaired CALVIN ABC training data, and CALVIN chain evaluator of the main CALVIN row, but trains for 4,000 steps at a constant learning rate of 6.25×10^{-6} .

C.5 Published LIBERO reference points and adapted-policy polish diagnostic

Table C.9 situates the benchmark settings against commonly reported LIBERO results from published VLA work, with the source and protocol context for each reference point noted in the table. The final block reports a short polish diagnostic from the released LeRobot $\pi_{0.5}$ LIBERO adapted checkpoint `lerobot/pi05_libero_finetuned`: its released-checkpoint evaluation, and a matched Baseline / FIBERTUNE pair continued to step 300 from that near-saturated checkpoint.

C.6 SO-101 trial breakdown

Table C.10 breaks down the 128 physical trials per arm by block color: yellow, orange, and purple are in-distribution colors from the 90-demonstration training set, and green is held out for color generalization. These rows give the per-color breakdown behind the aggregate results; the

Table C.7: Wilson 95% confidence intervals for success metrics.

Evaluation setting	Method	Metric	Value (%)	95% CI (%)
CALVIN / $\pi_{0.5}$ / general	Baseline	SR (5)	0.4	[0.2, 1.0]
CALVIN / $\pi_{0.5}$ / general	FIBERTUNE	SR (5)	1.3	[0.8, 2.2]
CALVIN / $\pi_{0.5}$ / adapted	SOURCE	SR (5)	62.3	[59.3, 65.3]
CALVIN / $\pi_{0.5}$ / adapted	Baseline	SR (5)	61.4	[58.3, 64.4]
CALVIN / $\pi_{0.5}$ / adapted	FIBERTUNE	SR (5)	72.1	[69.2, 74.8]
CALVIN / $\pi_{0.5}$ / adapted, 3-seed pooled	Baseline	SR (5)	62.1	[60.4, 63.9]
CALVIN / $\pi_{0.5}$ / adapted, 3-seed pooled	FIBERTUNE	SR (5)	70.9	[69.2, 72.5]
LIBERO / $\pi_{0.5}$ / general	Baseline	SR	92.35	[91.10, 93.44]
LIBERO / $\pi_{0.5}$ / general	FIBERTUNE	SR	93.35	[92.17, 94.36]
LIBERO / $\pi_{0.5}$ / adapted, seed 1000	Baseline	SR	95.75	[94.77, 96.55]
LIBERO / $\pi_{0.5}$ / adapted, seed 1000	FIBERTUNE	SR	97.10	[96.27, 97.75]
LIBERO / $\pi_{0.5}$ / adapted, 3-seed pooled	Baseline	SR	96.12	[95.60, 96.58]
LIBERO / $\pi_{0.5}$ / adapted, 3-seed pooled	FIBERTUNE	SR	96.82	[96.34, 97.23]
LIBERO / OpenVLA-OFT / general	Baseline	SR	42.50	[40.35, 44.68]
LIBERO / OpenVLA-OFT / general	FIBERTUNE	SR	48.95	[46.76, 51.14]
LIBERO / OpenVLA-OFT / adapted	Baseline	SR	95.35	[94.34, 96.19]
LIBERO / OpenVLA-OFT / adapted	FIBERTUNE	SR	96.15	[95.21, 96.91]
SO-101 / $\pi_{0.5}$ / all colors	Baseline	contact	93.8	[88.2, 96.8]
SO-101 / $\pi_{0.5}$ / all colors	FIBERTUNE	contact	96.9	[92.2, 98.8]
SO-101 / $\pi_{0.5}$ / all colors	Baseline	lift	81.2	[73.6, 87.1]
SO-101 / $\pi_{0.5}$ / all colors	FIBERTUNE	lift	82.8	[75.3, 88.4]
SO-101 / $\pi_{0.5}$ / all colors	Baseline	task success	72.7	[64.4, 79.6]
SO-101 / $\pi_{0.5}$ / all colors	FIBERTUNE	task success	78.1	[70.2, 84.4]
SO-101 / $\pi_{0.5}$ / ID colors	Baseline	task success	81.2	[72.3, 87.8]
SO-101 / $\pi_{0.5}$ / ID colors	FIBERTUNE	task success	83.3	[74.6, 89.5]
SO-101 / $\pi_{0.5}$ / held-out green	Baseline	task success	46.9	[30.9, 63.6]
SO-101 / $\pi_{0.5}$ / held-out green	FIBERTUNE	task success	62.5	[45.3, 77.1]

Table C.8: CALVIN low-learning-rate constant-schedule calibration point.

Starting checkpoint	Method	Step	Avg. seq. len.	SR (5) (%)	Trials
CALVIN adapted	Baseline	4,000	3.992	63.9	1000
CALVIN adapted	FIBERTUNE	4,000	4.206	71.5	1000

Table C.9: LIBERO reference points from published VLA results and an adapted-policy polish diagnostic. Values are success rates in percent over the four LIBERO suites when suite-level results are available.

Reference point	Spatial	Object	Goal	LIBERO-10	Avg.	Source / note
Diffusion Policy (scratch)	78.3	92.5	68.3	50.5	72.4	[21, 8]
Octo (fine-tuned)	78.9	85.7	84.6	51.1	75.1	[10, 8]
OpenVLA (fine-tuned)	84.7	88.4	79.2	53.7	76.5	[8]
π_0 + FAST (fine-tuned)	96.4	96.8	88.6	60.2	85.5	[22, 12, 9]
π_0 (fine-tuned)	96.8	98.8	95.8	85.2	94.2	[12, 9]
OpenVLA-OFT with additional inputs	97.6	98.4	97.9	94.5	97.1	[9]
GR00T N1.5	98.2	99.4	97.2	87.8	95.7	[40, 24]
GR00T N1.5 + RS-CL	98.4	98.6	98.2	90.4	96.4	[24, 40]
$\pi_{0.5}$ adapted source lerobot/pi05-libero_finetuned	98.4	99.0	96.0	95.4	97.20	Released checkpoint evaluation
$\pi_{0.5}$ adapted polish Baseline	97.6	99.0	97.6	95.2	97.35	Step 300
$\pi_{0.5}$ adapted polish FIBERTUNE	97.6	99.2	97.8	96.0	97.65	+0.30 pp / +0.31% vs Baseline

in-distribution colors remain high overall, and the held-out green condition shows the largest task-success gain.

Table C.10: SO-101 physical trial breakdown by color. Entries report successes out of 32 trials per color, with percentages in parentheses.

Color	Split	Method	Contact	Lift	Task success
Yellow	ID	Baseline	30/32 (93.8)	25/32 (78.1)	25/32 (78.1)
Yellow	ID	FIBERTUNE	32/32 (100.0)	28/32 (87.5)	26/32 (81.2)
Orange	ID	Baseline	32/32 (100.0)	29/32 (90.6)	26/32 (81.2)
Orange	ID	FIBERTUNE	32/32 (100.0)	29/32 (90.6)	28/32 (87.5)
Purple	ID	Baseline	31/32 (96.9)	27/32 (84.4)	27/32 (84.4)
Purple	ID	FIBERTUNE	32/32 (100.0)	26/32 (81.2)	26/32 (81.2)
Green	OOD	Baseline	27/32 (84.4)	23/32 (71.9)	15/32 (46.9)
Green	OOD	FIBERTUNE	28/32 (87.5)	23/32 (71.9)	20/32 (62.5)